Supporting Information

Transformation of Hydride-Containing Dinitrosyl Iron Complex $[(NO)_2Fe(\eta^2\text{-}BH_4)]^-$ into $[(NO)_2Fe(\eta^3\text{-}HCS_2)]^-$ via Reaction with CS_2

Huang-Chia Huang,[a] Wei-Min Ching,[b] Yu-Ting Tseng,[a,c] Chien-Hong Chen,*[d] and Tsai-Te Lu*[a,e]

Affiliations:

[a]Department of Chemistry, Chung Yuan Christian University, Taoyuan, 32023, Taiwan.

[b]Instrumentation Center, National Taiwan Normal University, Taipei, 106, Taiwan

[c]Department of Chemistry, National Tsing Hua University, Hsinchu, 30013, Taiwan.

[d]Department of Medical Applied Chemistry, Chung Shan Medical University and Department of Medical Education, Chung Shan Medical University Hospital, Taichung 40201, Taiwan

[e]Institute of Biomedical Engineering, National Tsing Hua University, Hsinchu, 30013, Taiwan.

**To whom correspondence should be addressed*

E-mail: cchwind@csmu.edu.tw (C.-H.C.); ttlu@mx.nthu.edu.tw (T.-T.L.)

Experimental Section.

Manipulations, reactions, and transfers were conducted under $N_{2(g)}$ according to Schlenk techniques or in a glovebox (under $N_{2(g)}$ atmosphere). Organic solvents were distilled under $N_{2(g)}$ from appropriate drying agents (acetonitrile (CH_3CN) and dichloromethane (CH_2Cl_2) from CaH_2; n-hexane, diethyl ether, and tetrahydrofuran (THF) from sodium benzophenone) and stored in dried, N_2-filled flasks over 4 Å molecular sieves. Nitrogen was purged through these solvents before use. Solvent was transferred to the reaction vessel via stainless cannula under positive pressure of N_2. Compounds [PPN][$^{15}NO_2$], [^{15}NO][BF_4],[1] [PPN][$Fe(CO)_3(^{15}NO)$],[2] [$(NO)_2Fe$(TMEDA)] (TMEDA = tetramethylenediamine), [$(^{15}NO)_2Fe$(TMEDA)],[3] and NaS_2CH[4] were prepared according to the reported procedures. The reagents 18-crown-6-ether (Alfa Aesar), TMEDA (Alfa Aesar), sodium borohydride/borodeuteride (Alfa Aesar), ammonia borane (Sigma), 9-borabicyclononane (9-BBN) (ACROS), pinacolborane (Alfa Aesar), borane tetrahydrofuran complex solution (Aldrich), and carbon disulfide (Sigma) were used as received. Infrared spectra of the ν_{NO} and $\nu_{B\text{-}H/D}$ stretching frequencies were recorded on a JASCO FT/IR-4200 spectrometer with sealed solution cells (0.1 mm, CaF_2 windows). UV-vis spectra were recorded on a JASCO V-630 spectrometer. ^1H, ^{11}B, ^{13}C, and ^{15}N NMR spectra were obtained on a Bruker AVANCE 300 MHz and Varian Unity-600 MHz spectrometer, whereas BF_3 (δ = 0 ppm) and urea (δ = -298.73 ppm) were used as external standard for ^{11}B and ^{15}N NMR, respectively. All electrochemical measurements were performed in a three-electrode cell with a CHI model 611E potentiostat (CH Instrument) instrumentation. Cyclic voltammogram of dinitrosyl iron complex was obtained in O_2-free THF using 0.1 M [*n*-Bu_4N][PF_6] as the supporting electrolyte. The potential was measured at 298 K vs $Ag/AgNO_3$ reference electrode (0.01 M $AgNO_3$) using a glassy carbon working

electrode (surface area = 0.0707 cm^2) and a platinum wire auxiliary electrode at a scan rate of 0.1 V/s. The potentials are reported against the ferrocenium/ferrocene (Fc^+/Fc) couple.

Reaction of Complex [$(NO)_2$Fe(TMEDA)] (1) and NH_3BH_3, BH_3 • THF, 9-BBN (9-borabicyclononane), and HBPin (pinacolborane), respectively. Compounds [$(NO)_2$Fe(TMEDA)] (**1**) (0.023 g, 0.1 mmol) and NH_3BH_3 (0.015 g, 0.5 mmol) were dissolve in THF (5 mL) and then stirred under N_2 at ambient temperature for 12 h. No change of indicative IR ν_{NO} stretching frequencies of complex **1** at 1697 s, 1644 s cm^{-1} demonstrated that complex **1** is unreactive toward NH_3BH_3. Reactions of complexes **1** with BH_3 • THF, 9-BBN, and HBPin, respectively, as well as reactions of complex [$(NO)_2Fe(CO)_2$] with NH_3BH_3/BH_3 • THF/9-BBN/HBPin were carried out in a similar fashion, while no reaction was observed.

Preparation of [Cation][$(NO)_2$Fe(η^2-BH_4)] (2) (Cation = Na-18-crown-6-ether or PPN). A 25-mL Schlenk tube was loaded with compounds [$(NO)_2$Fe(TMEDA)] (**1**) (0.278 g, 1.2 mmol), $NaBH_4$ (0.038 g, 1.0 mmol) and 18-crown-6-ether (0.264 g, 1.0 mmol), and the contents in the tube were dissolved in THF (5 mL). The reaction solution was stirred at ambient temperature under $N_{2(g)}$ atmosphere for 1 h and then the mixture solution was filtered through Celite to remove the insoluble solid. Hexane was further added to the filtrate to precipitate the dark-brown solid. The dark-brown solid was washed with diethyl ether (25 mL) to remove the excess complex [$(NO)_2$Fe(TMEDA)] (**1**). After drying the resulting dark-brown solid under vacuum, the dark-brown complex [Na-18-crown-6-ether][$(NO)_2$Fe(η^2-BH_4)] (**2-Na**) (yield 0.31 g, 73.5%) was afforded. Recrystallization from THF solution of complex **2** layered with hexane at -20 °C for a week led to dark-brown crystals suitable for X-ray crystallography. IR ν_{NO}: 1708 s, 1654 s cm^{-1} (THF); 1714 s, 1651 s cm^{-1} (KBr). ^{1}H

NMR (300 MHz, d-THF, 298 K) δ 3.62 (s, 24H, 18-crown-6-ether), -2.13 (q, 4H, BH_4, $^1J_{BH}$ = 84 Hz) ppm. ^{15}N NMR (61 MHz, d-THF) δ 10.21 ppm. Absorption spectrum (THF) [λ_{max}, nm (ε, $M^{-1}cm^{-1}$)]: 327 (890), 388 (785).

Complex [PPN][$(NO)_2Fe(\eta^2\text{-}BH_4)$] (**2-PPN**) was prepared in a similar manner through the reaction of complex **1** and [PPN][BH_4]**.** IR ν_{NO}: 1707 s, 1653 s cm^{-1} (THF); 1714 s, 1651 s cm^{-1} (KBr). ^1H NMR (300 MHz, d-THF, 298 K) δ 7.68 (s, 6H, PPN), 7.59 (s, 12H, PPN), 7.51 (s, 12H, PPN), -2.08 (q, 4H, BH_4, $^1J_{BH}$ = 84 Hz) ppm. ^1H NMR (600 MHz, d-THF, 213 K) δ 7.68 (s, 6H, PPN), 7.59 (s, 12H, PPN), 7.51 (s, 12H, PPN), 3.71 (s, 2H, B-H_t), -7.96 (s, 2H, B-H_b) ppm. ^{11}B NMR (192 MHz, THF) δ 2.82 (q, $^1J_{BH}$ = 84.5 Hz) ppm.

Deuterium-substituted complex [18-crown-6-ether][$(NO)_2Fe(\eta^2\text{-}BD_4)$] (**2-D**) was prepared in a similar manner through the reaction of complex **1**, 18-crown-6-ether, and $NaBD_4$**.**

Preparation of [18-crown-6-ether][$(NO)_2Fe(\eta^3\text{-}HCS_2)$] (3). Method 1. Complex **2-Na** (0.125 g, 0.3 mmol) was dissolve in THF (5 mL) before CS_2 (18 μl, 0.3 mmol) was added in a dropwise manner to this THF solution. The reaction solution was then stirred under $N_{2(g)}$ at ambient temperature for 2 h and monitored with FTIR. Shift of IR ν_{NO} stretching frequencies from 1708 s and 1654 vs cm^{-1} to 1717 s and 1648 s cm^{-1} was observed. Subsequent addition of diethyl ether to this THF solution led to the precipitation of [Na-18-crown-6-ether][$(NO)_2Fe(\eta^3\text{-}HCS_2)$] (**3**) (yield: 0.063 g, 43.5 %)

.

Method 2. A 25-mL Schlenk tube was loaded with 18-crown-6-ether (0.264 g, 1.0 mmol)) and NaS_2CH (0.100 g, 1.0 mmol) and the contents in the tube were dissolved in THF (5 mL). The mixture solution was stirred for 1 h and then transferred by cannula under positive N_2 pressure to another 25-mL Schlenk tube loaded with

complex **1** (0.232 g, 1.0 mmol). The reaction solution was stirred for 4 h and then monitored by FTIR spectroscopy, which indicated the formation of [Na-18-crown-6-ether][$(NO)_2Fe(\eta^3\text{-}HCS_2)$]. The mixture was filtered through Celite to remove the insoluble solid before hexane was added to precipitate the dark-brown solid of [Na-18-crown-6-ether][$(NO)_2Fe(\eta^3\text{-}HCS_2)$] (**3**) (yield: 0.351 g, 73.2 %). Recrystallization from THF solution of complex **3** layered with hexane at -20 °C for a week led to dark-brown crystals suitable for X-ray crystallography. IR ν_{NO}: 1717 s, 1648 s cm^{-1} (THF); 1717 s, 1639 s cm^{-1} (KBr). ^1H NMR (600 MHz, d-THF, 298 K) δ 7.93 (s, 1H, HCS_2), δ 3.61 (s, 24H, 18-crown-6-ether). ^{15}N NMR (61 MHz, d-THF) δ 74.71 ppm. Absorption spectrum (THF) [λ_{max}, nm (ε, $M^{-1}cm^{-1}$)]: 334 (4650), 366 (3770), 418 (2150).

Reaction of Complex 2 and CO_2. To a 5-mL THF solution of complex **2-PPN** (0.067 g, 0.1 mmol), dry CO_2 was purged for 5 min before this reaction solution was monitored by with FTIR. Disappearance of the IR ν_{NO} stretching frequencies at 1708 and 1654 cm^{-1} indicated the decomposition of complex **2**. Solvent was then removed under vacuum, whereas the crude solid was extracted with CD_3CN. The singlet ^1H NMR signal observed at 8.29 ppm as well as the ^{13}C NMR signal observed at 164.47 ppm indicated the formation of $[HB(HCOO)_3]^-$ (yield 66.8% using CH_2Cl_2 as an internal standard).

Conversion of Complex 2 into Complex 1 via Reaction with CO_2 in the presence of TMEDA. Dry CO_2 was purged through a 5-mL THF solution of complex **2** (0.042 g, 0.1 mmol) and TMEDA (1.7 μl, 0.1 mmol) for 5 min. The reaction solution was stirred for an additional 1 h and a significant change in color of the reaction solution from red to deep green was observed. The reaction was then monitored with FTIR. Shift of IR ν_{NO} stretching frequencies from 1708 s and 1654 vs cm^{-1} to 1697 s and 1644 s cm^{-1} was assigned to the conversion of complex **2** into complex **1**.

Crystallography. Dark-brown crystals of complexes [Na-18-crown-6-ether][$(NO)_2Fe(\eta^2\text{-}BH_4)$] (**2-Na**) and [Na-18-crown-6-ether][$(NO)_2Fe(\eta^3\text{-}HCS_2)$] (**3**) suitable for single-crystal X-ray diffraction were mounted, respectively, on a glass fiber and quickly coated in epoxy resin. Unit cell parameters were obtained by least-squares refinement. Diffraction measurement for complexes **2-Na** and **3** were carried out on a SMART Apex CCD diffractometer with graphite monochromated Mo Kα radiation (λ = 0.71073 Å) and between 2.52˚ and 27.47˚ for complex **2-Na**, and between 2.37˚ and 24.95˚ for complexes **3**. Least-squares refinement of the positional and anisotropic thermal parameters of all non-hydrogen atoms and fixed hydrogen atoms was based on F^2. A SADABS absorption correction was made.[5] The SHELXTL structure refinement program was employed.[6] Crystallographic data of DNICs **2-Na** (CCDC 1881645) and **3** (CCDC 1881646) were deposited in Cambridge Crystallographic Data Centre.

Computational methods. Geometry optimization of complexes **1**, **2**, and **3**, directly adopted from single-crystal structures, was achieved using Gaussian 09 program with PB86/TZVP and B3LYP/TZVP levels.[7] The geometry-optimized structures with BP86 method are consistent with the single-crystal structures (Table S2), whereas no imaginary frequencies were observed. Extended transition state nature orbital for the chemical valence (ETS-NOCV) analysis[8-13] were performed with BP86/TZVP method using Amsterdam Density Function (ADF) software package[14]. The deformation density plots of all results were plotted with Chimera program.[15]

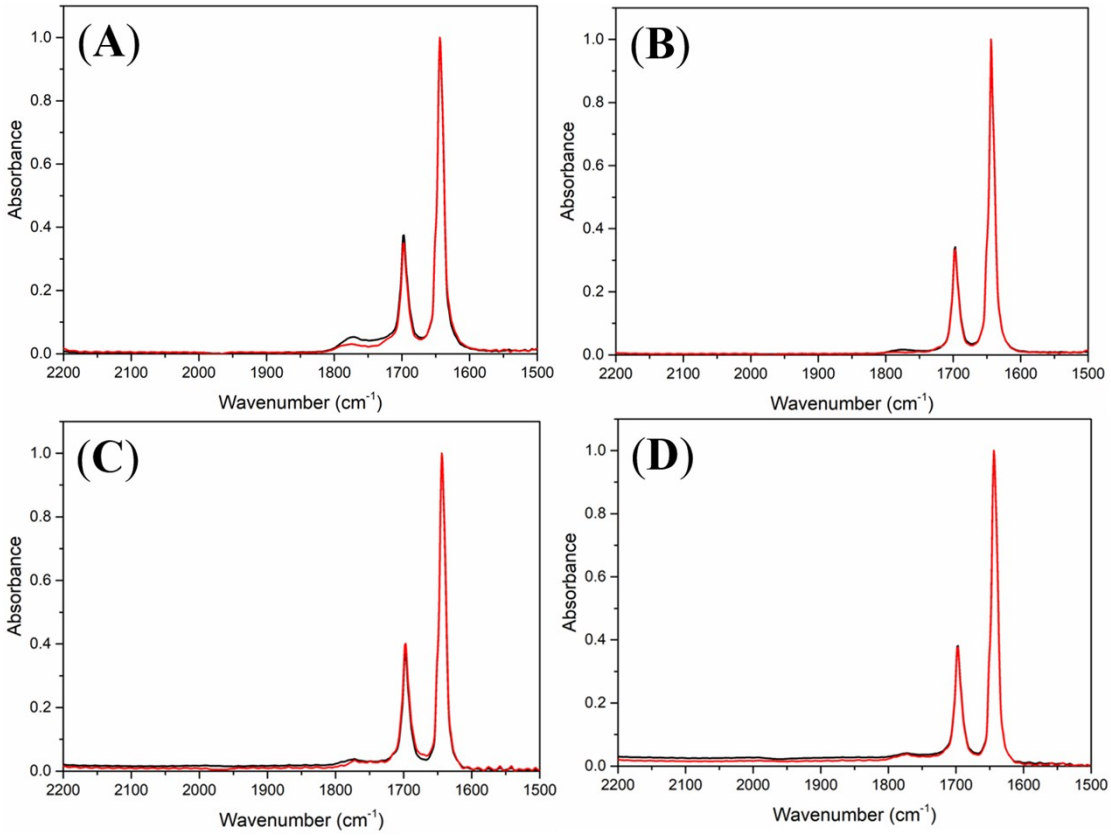

Figure S1. IR spectra of DNIC **1** in THF (black) and its reaction with five equiv. of (**A**) NH_3BH_3, (**B**) BH_3 • THF, (**C**) 9-BBN, and (**D**) HBPin, respectively, for 12 h (red).

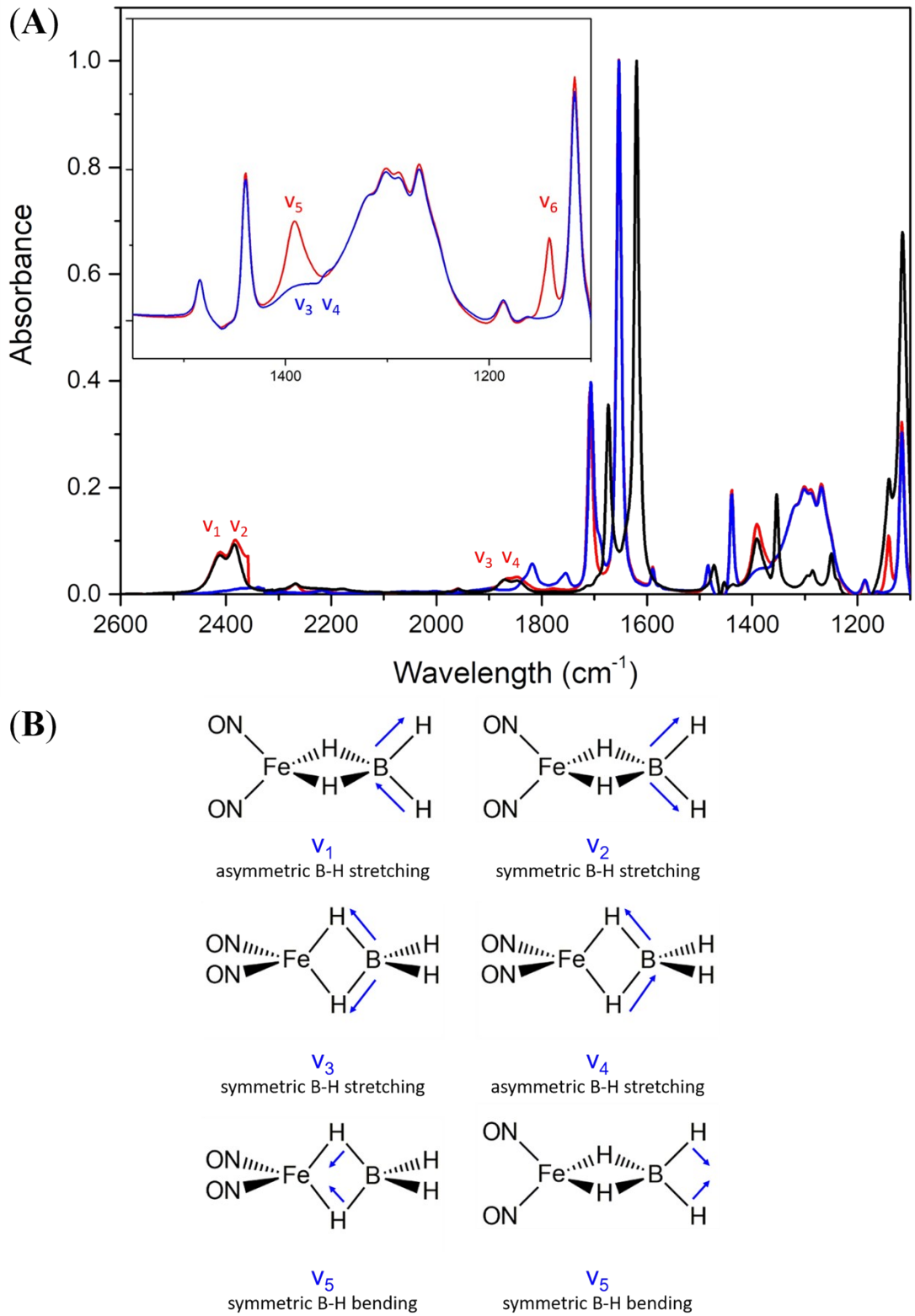

Figure S2. (**A**) IR spectra of DNICs [Na-18-crown-6-ether][$(NO)_2Fe(\eta^2\text{-}BH_4)$] (**2**) (red), [Na-18-crown-6-ether][$(NO)_2Fe(\eta^2\text{-}BD_4)$] (**2-D**) (blue), and [Na-18-crown-6-ether][$(^{15}NO)_2Fe(\eta^2\text{-}BH_4)$] (black) in THF. The comparison of the IR spectra of DNICs **2** (red), **2-D** (blue) in the range between 1100-1550 cm^{-1} is shown in the inset. (**B**) Vibrational modes of the $[BH_4]^-$ ligand in DNIC **2** identified by isotope-labeling experiment and theoretical calculation.

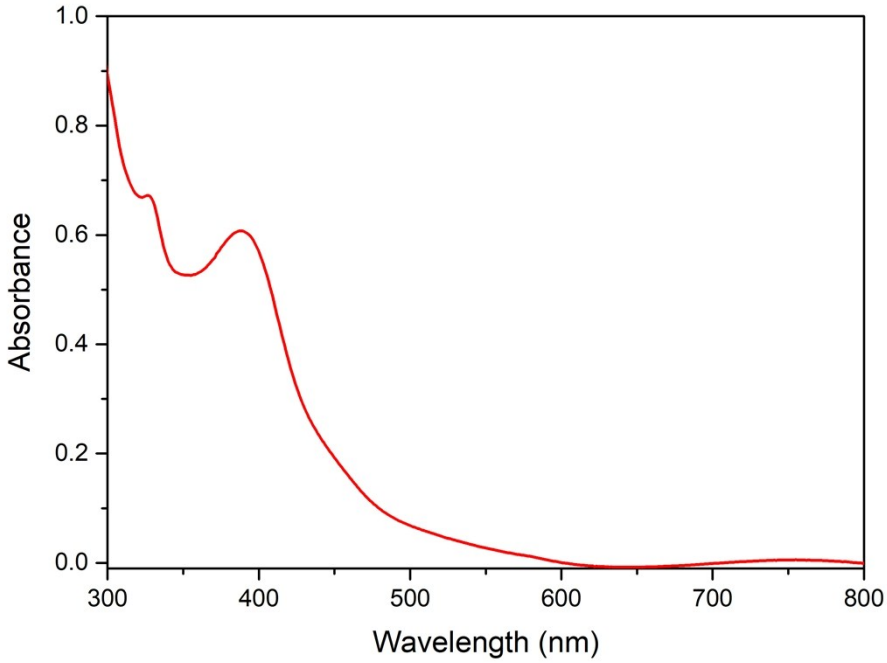

Figure S3. UV-vis spectrum DNIC **2** in THF.

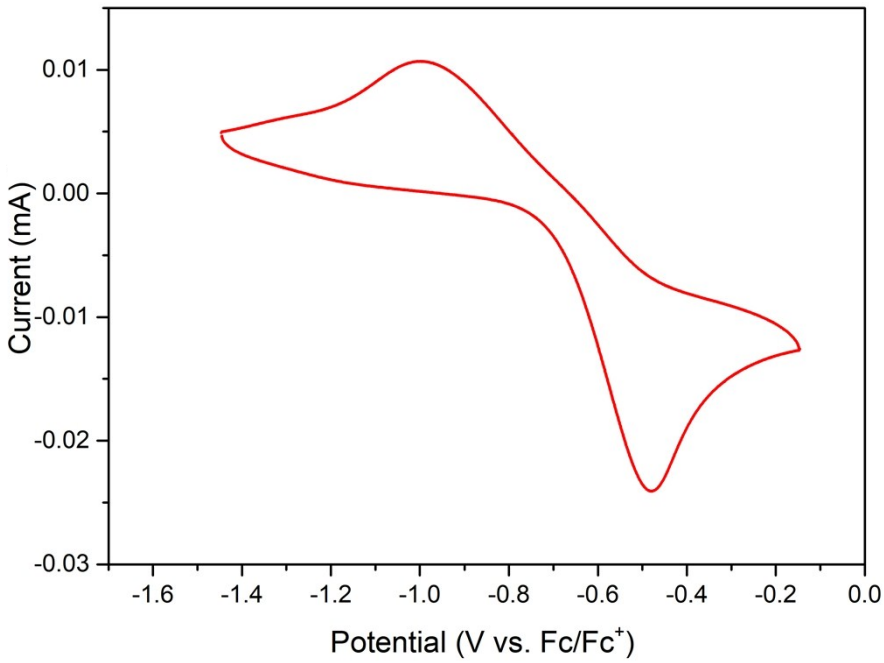

Figure S4. Cyclic voltammogram of 2-mM solution of DNIC **2** in THF with 0.1 M of [n-Bu_4N][PF_6] electrolyte indicate the oxidation of DNIC **2** at E_{pa} = -0.48 V versus Fc/Fc^+.

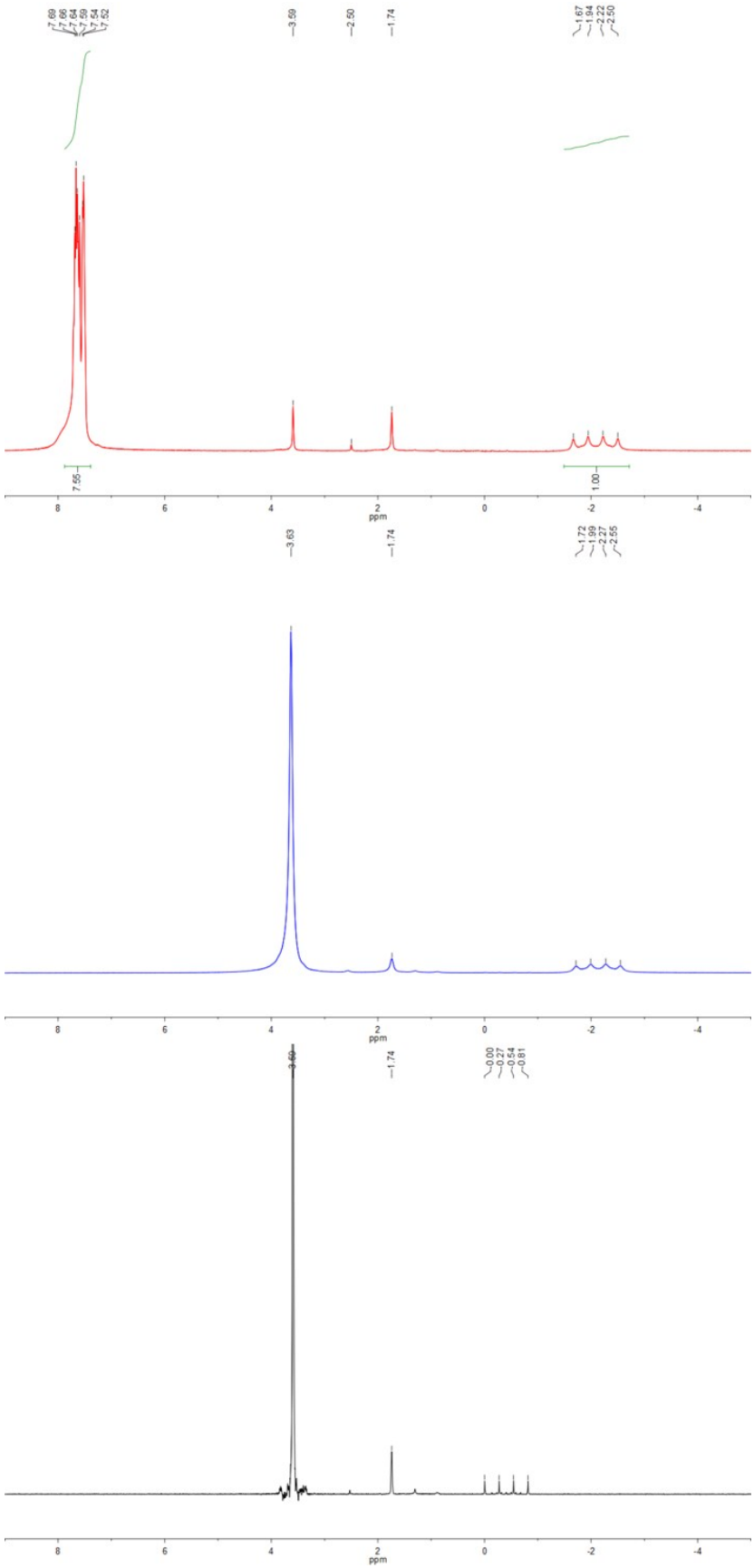

Figure S5. ^{1}H NMR spectra of DNICs **2-PPN** (red), **2** (blue), and compound [Na-18-crown-6-ether][BH_4] (black) in d-THF at 298 K.

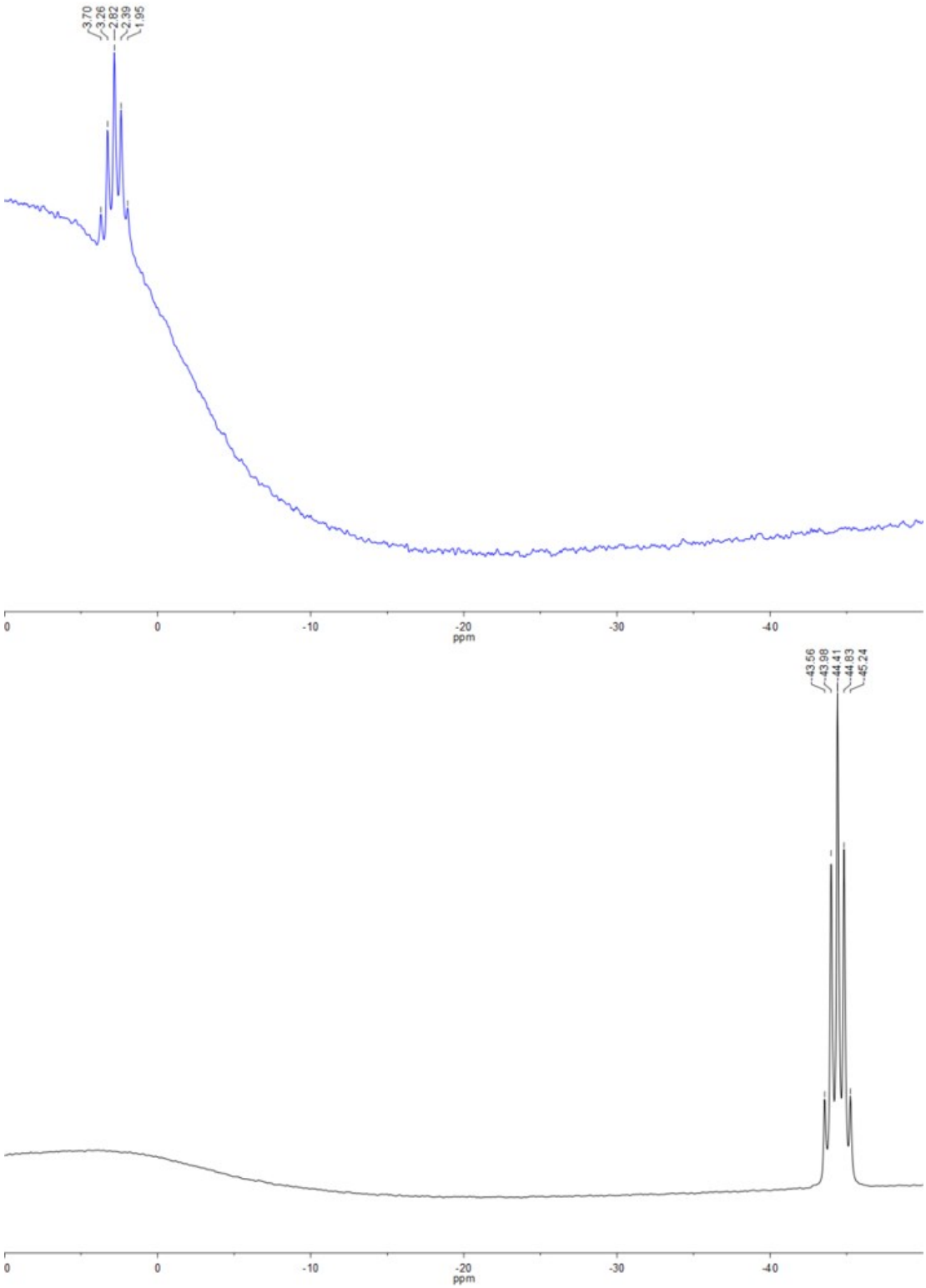

Figure S6. ^{11}B NMR spectra of DNIC **2** (blue) and compound [Na-18-crown-6-ether][BH_4] (black) in d-THF at 298 K.

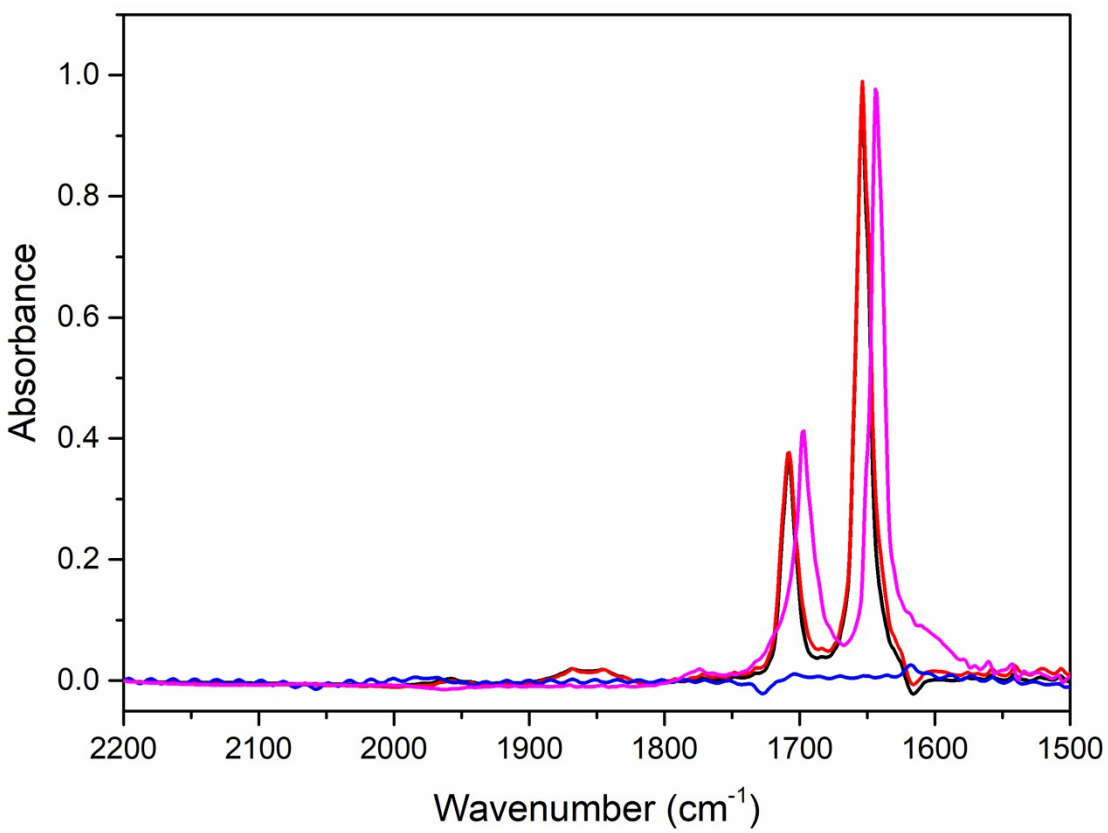

Figure S7. IR spectra of DNIC **2** in THF (black), its reaction with five equiv. of TMEDA for 12 h (red), its reaction with $CO_{2(g)}$ (blue), and its reaction with $CO_{2(g)}$ in the presence of one equiv. of TMEDA (magenta).

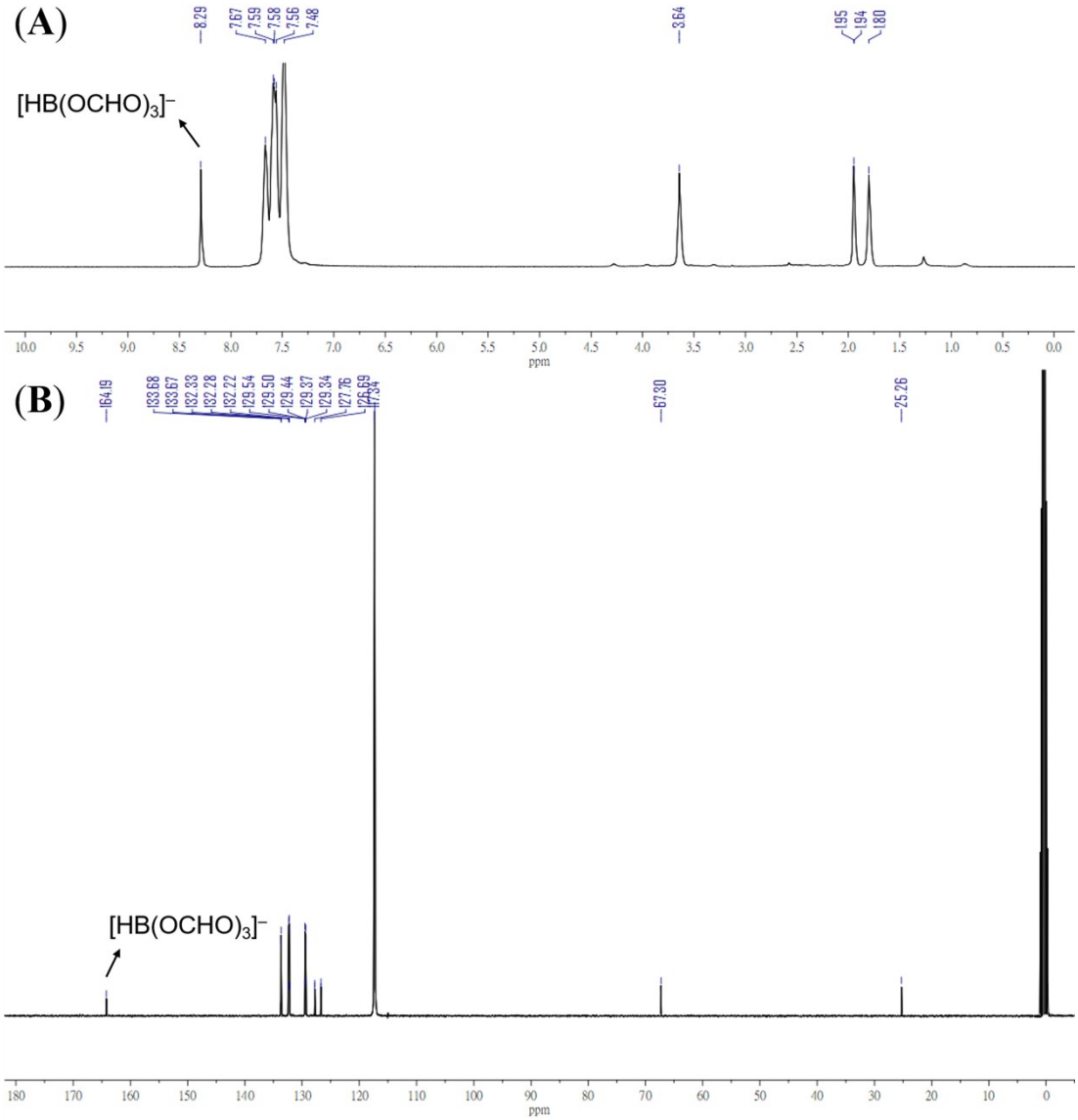

Figure S8. (**A**) ^{1}H NMR and (**B**) ^{13}C NMR NMR spectra for the CD_3CN solution of complex **2-PPN** purged with $CO_{2(g)}$ for 10 min at 298 K.

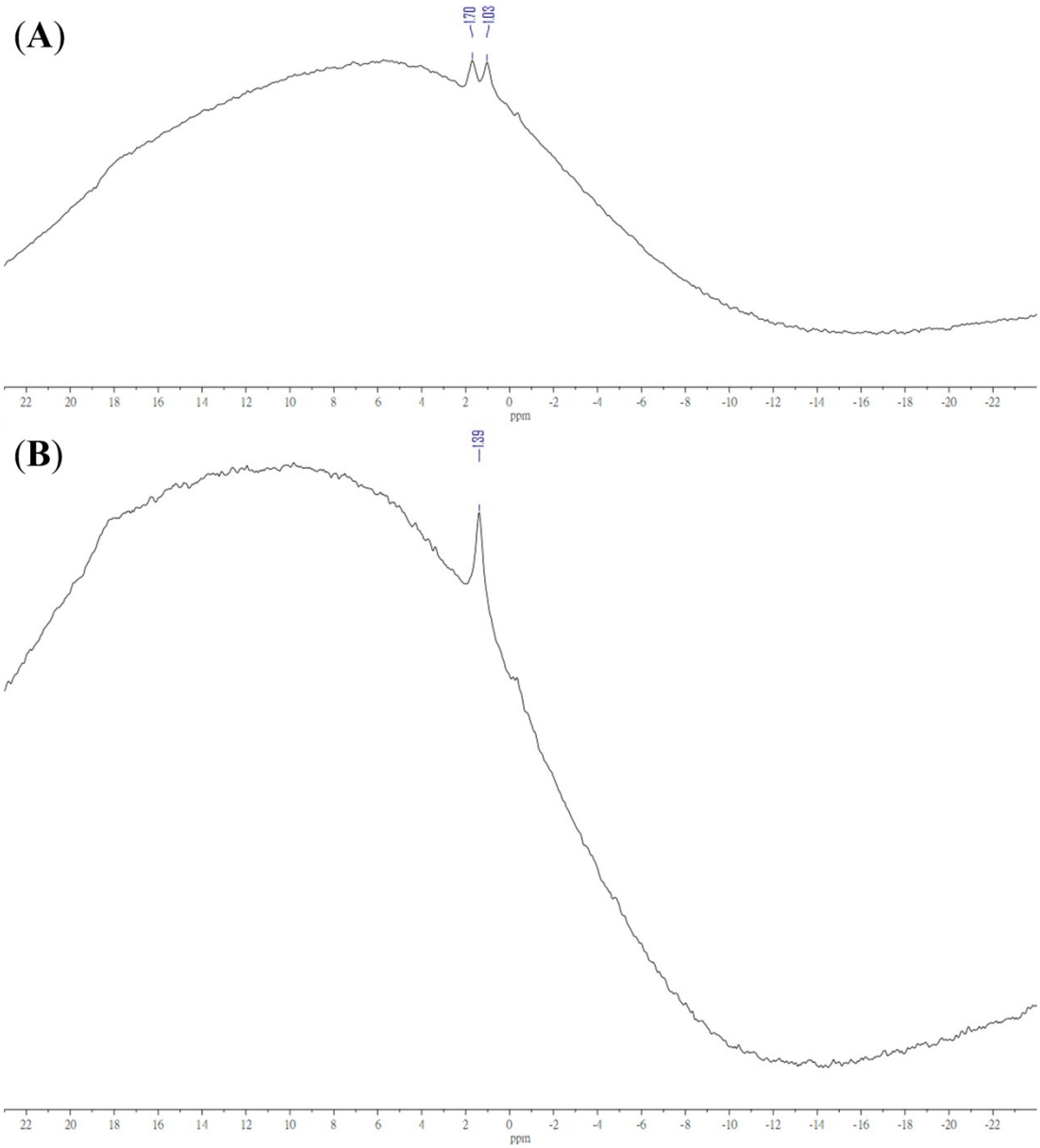

Figure S9. (**A**) ^{11}B NMR, and (B) $^{11}B\{H\}$ NMR spectra for the CD_3CN solution of complex **2-PPN** purged with $CO_{2(g)}$ for 10 min at 298 K.

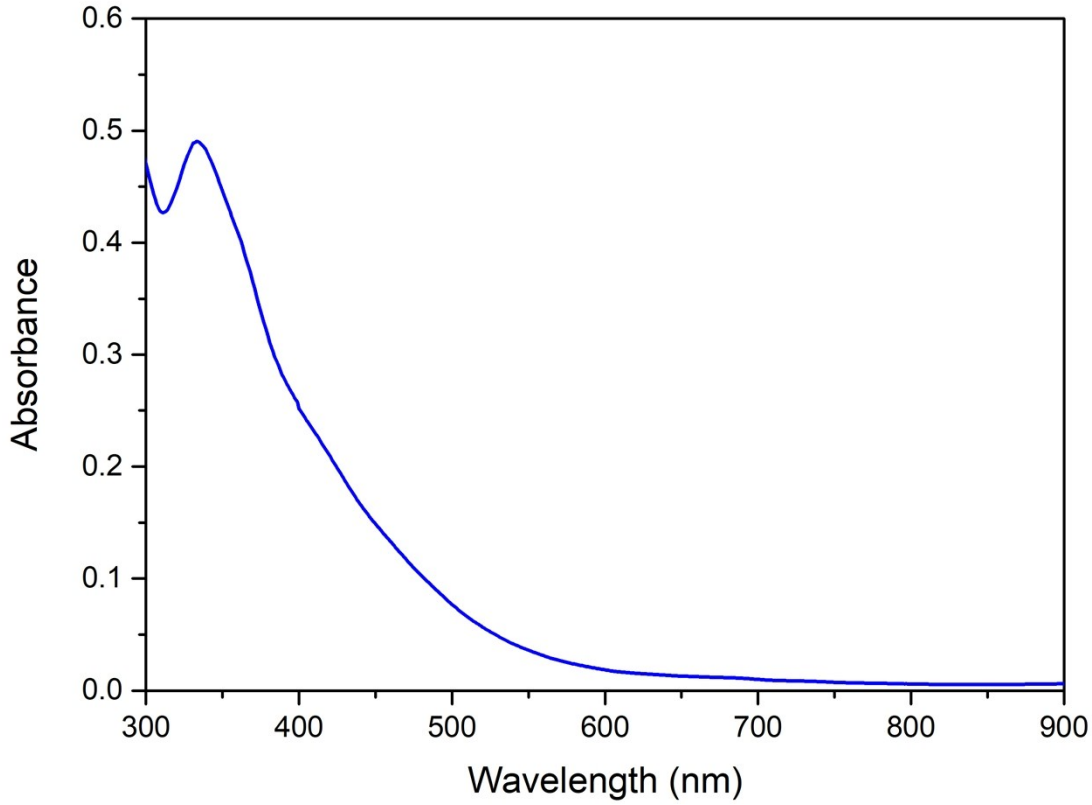

Figure S10. UV-vis spectrum DNIC **3** in THF.

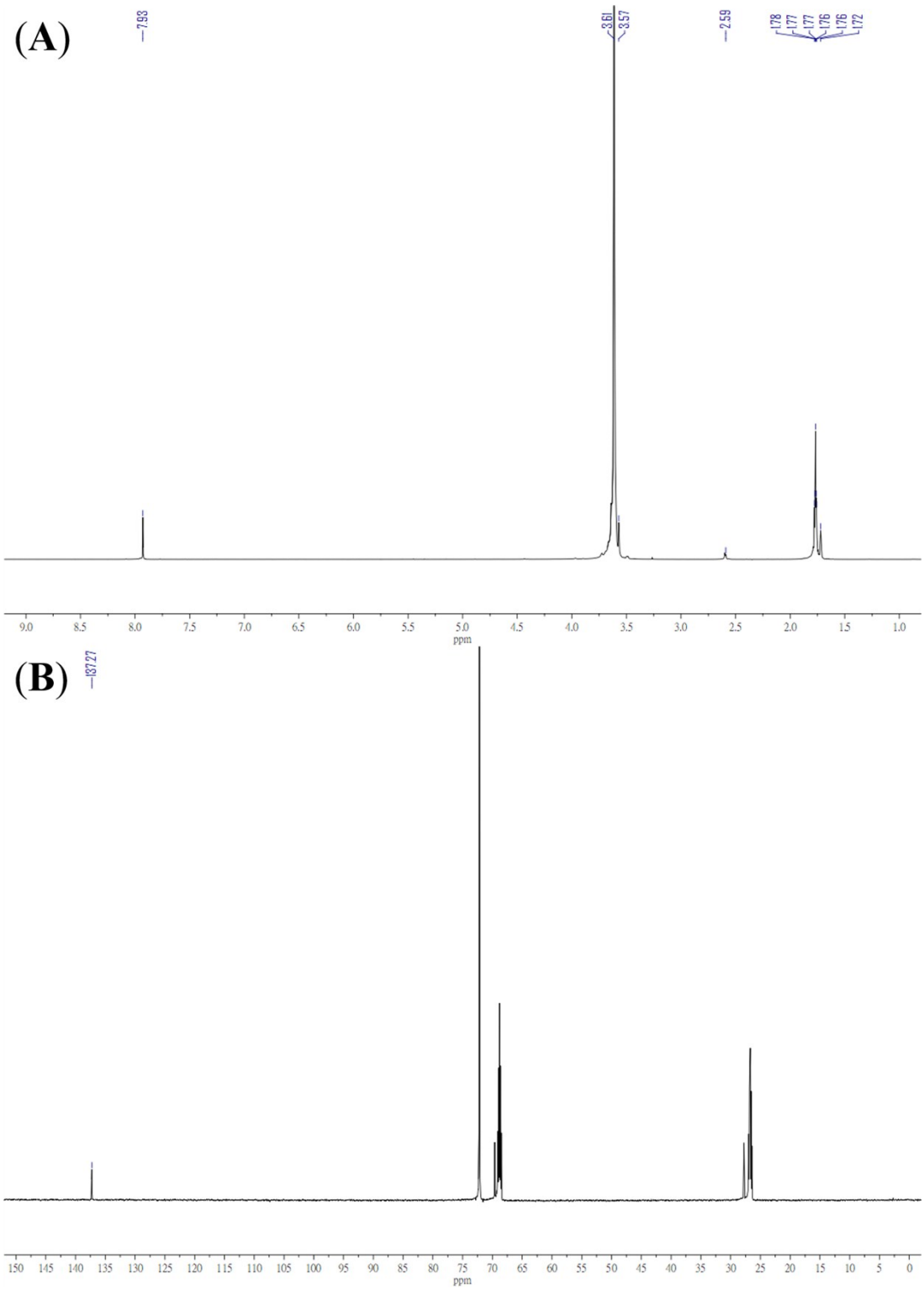

Figure S11. (**A**) ^{1}H NMR and (**B**) ^{13}C NMR spectra of DNIC **3** in d-THF at 298 K.

Table S1. Experimental and Calculated Vibrational Frequencies for Different Vibrational Modes of the $[BH_4]^-$ ligand in DNIC **2**.

Vibrational Modes	Vibrational Frequency (cm^{-1})			
	Experimental (in THF)		Calculated[b]	
	^1H	^2D	^1H	^2D
[a]asym. B-H_t stretching (ν_1)	2410	1818	2475	1845
[a]sym. B-H_t stretching (ν_2)	2382	1754	2443	1799
[a]sym. B-H_b stretching (ν_3)	1865	1382	1979	1424
[a]asym. B-H_b stretching (ν_4)	1847	1358	1937	1431
B-H_b bending (ν_5)	1391	-	1450	1048
B-H_t bending (ν_6)	1141	-	1179	873

[a]asym. = asymmetric; sym. = symmetric. [b]with BP86/TZVP level.

Table S2. Selected Bond Distances, Bond Angle, and IR ν_{NO} Stretching Frequencies for DNICs **1**, **2**, and **3** Obtained from Single-crystal Structure and Geometry Optimization.

Single-Crystal Structures	Fe–NO (Å)	N–O (Å)	∠Fe–N–O	Fe–N (Å)	Fe–B (Å)	Fe–C (Å)	Fe–S (Å)	IR ν_{NO} (cm^{-1})
1	1.638	1.197	166.8	2.110	-	-	-	1697
	1.639	1.188	169.8	2.117				1644
2	1.627	1.149	170.8	-	2.194	-	-	1708
	1.661	1.180	174.8					1654
3	1.677	1.189	155.1	-	-	2.070	2.297	1717
	1.641	1.190	177.2				2.294	1648
BP86/TZVP	Fe–NO (Å)	N–O (Å)	∠Fe–N-O	Fe–N (Å)	Fe–B (Å)	Fe–C (Å)	Fe–S (Å)	IR ν_{NO} (cm^{-1})
1	1.644	1.198	169.3	2.146	-	-	-	1727
	1.644	1.198	169.3	2.145				1678
2	1.641	1.204	168.4	-	2.159	-	-	1707
	1.641	1.204	168.4					1655
3	1.673	1.204	149.7	-	-	2.070	2.332	1732
	1.642	1.194	176.6				2.332	1634
B3LYP/TZVP	Fe–NO (Å)	N–O (Å)	∠Fe–N-O	Fe–N (Å)	Fe–B (Å)	Fe–C (Å)	Fe–S (Å)	IR ν_{NO} (cm^{-1})
1	1.631	1.185	170.0	2.160	-	-	-	1794
	1.631	1.185	170.0	2.159				1725
2	1.625	1.190	168.1	-	2.183	-	-	1773
	1.625	1.190	168.1					1700
3	1.647	1.188	154.0	-	-	2.094	2.364	1794
	1.624	1.180	179.8				2.364	1701

Table S3. Selected Bond Distances, Bond Angle, and IR ν_{NO} Stretching Frequencies for Neutral $\{Fe(NO)_2\}^{10}$ DNICs Containing CO/Carbene Ligands and (Di)Anionic $\{Fe(NO)_2\}^{10}$ DNICs.

Complex	Fe–NO (Å)	N–O (Å)	∠Fe–N-O	Fe–N (Å)	Fe–B (Å)	Fe–C (Å)	Fe–S (Å)	IR ν_{NO} (cm^{-1})	Ref.
1	1.639	1.193	168.3	2.114	-	-	-	1697 1644	This work
2	1.644	1.165	172.8	-	2.194	-	-	1708 1654	This work
3	1.677 1.641	1.189 1.190	155.1 177.2	-	-	2.070	2.296	1717 1648	This work
Neutral $\{Fe(NO)_2\}^{10}$ DNICs Containing CO/Carbene Ligands									
Complex	Fe–NO[c] (Å)	N–O[d] (Å)	∠Fe–N-O	Fe–CO (Å)	Fe–P (Å)	Fe–C[e] (Å)		IR ν_{NO} (cm^{-1})	Ref.
$[Fe_2(\mu\text{-}L_1)(NO)_4(CO)_2]$[a]	1.682	1.173	176.2	1.763	2.262	-		1760 1702	16
$[Fe_2(\mu\text{-}L_2)(NO)_4(CO)_2]$[a]	1.707	1.166	177.0	1.778	2.270	-		1767 1716	16
$[(IMes)(CO)Fe(NO)_2]$[a]	1.676	1.174	175.2	1.777	-	1.989		1744 1702	17
$[(NHC\text{-}Me)(CO)Fe(NO)_2]$[a]	1.727	1.176	173.2	1.729	-	2.025		1740 1697	18
$[(NHC\text{-}iPr)(CO)Fe(NO)_2]$[a]	1.676	1.181	175.8	1.784	-	2.005		1738 1696	18
$[(MeMes\text{-}NHC)(CO)Fe(NO)_2]$[a]	1.661	1.179	174.8	1.834	-	1.990		1743 1690	19
$[(sIMes)(CO)Fe(NO)_2]$[a]	1.683	1.169	172.6	1.771	-	1.998		1747 1705	20
$[(MeMes\text{-}NHC)_2Fe(NO)_2]$[a]	1.651	1.204	172.2	-	-	1.989		1675 1634	19
$[(NHC\text{-}Me)_2Fe(NO)_2]$[a]	1.660	1.202	174.0	-	-	1.973		1667 1624	18
$[(NHC\text{-}iPr)_2Fe(NO)_2]$[a]	1.643	1.204	173.8	-	-	2.015		1664 1619	18
(Di)Anionic $\{Fe(NO)_2\}^{10}$ DNICs									
	Fe–NO[c] (Å)	N–O[d] (Å)	∠Fe–N-O	Fe–N (Å)	Fe–O (Å)	Fe–P (Å)	Fe–S[f] (Å)	IR ν_{NO} (cm^{-1})	Ref.
$[(NO_2)(PPh_3)Fe(NO)_2]^-$	1.657	1.206	171.9	2.025	-	2.248	-	1693 1642	21
$[(NO)_2Fe(NC_9H_6\text{-}NH)]^-$[b]	1.622	1.183	168.8	2.048	-	-	-	1655 1603	22
$[(NO)_2Fe(NC_9H_6\text{-}O)]^-$[b]	1.620	1.231	169.7	2.045	2.021	-	-	1674 1619	22
$[(NO)_2Fe(NC_9H_6\text{-}S)]^-$[b]	1.652	1.209	170.2	2.067	-	-	2.316	1660 1612	22
$[(NO)_2Fe(SC_6H_4\text{-}o\text{-}NH_2)]^-$[b]	1.647	1.200	168.6	2.085	-	-	2.327	1657 1607	22
$[(NO)_2Fe(SC_2H_5)]^{2-}$[b]	1.642	1.205	167.8	-	-	-	2.324	1614 1571	23
$[(NO)_2Fe(S(CH_2)_3S)]^{2-}$[b]	1.650	1.217	168.7	-	-	-	2.331	1600 1552	13
$[(NO)_2Fe(S(CH_2)_2S)]^{2-}$[b]	1.650	1.218	167.4	-	-	-	2.329	1600 1559	13

[a] L_1 = bis(diphenylphosphino)methane (dppm); L_2 = bis(diphenylphosphino)acetylene (dppa); IMes = 1,3-bis(2,4,6-rimethylphenyl)imidazol-2-ylidene; NHC-Me = 1,3-dimethylimidazol-2-ylidene; NHC-iPr = 1,3-diisopropylimidazol-2-ylidene; MeMes-NHC = 1-methel-3-(2,4,6-trimethylphenyl)imidazol-2-ylidene; sIMes = 1,3-bis(2,4,6-trimethylphenyl)imidazol-2-ylidene. [b] The counteraction is [K-18-crown-6-ether]. [c] The average Fe–NO bond distance of neutral $\{Fe(NO)_2\}^{10}$ DNICs lies in the range of 1.638-1.727 Å, whereas that of (di)anionic $\{Fe(NO)_2\}^{10}$ DNICs lies in the range of 1.620-1.657 Å.[24] [d] The average N–O bond distance of $\{Fe(NO)_2\}^{10}$ DNICs without π-acceptor CO ligands lies in the range of 1.183-1.231 Å. [e] The average Fe–C(carbine) bond distance of neutral $\{Fe(NO)_2\}^{10}$ DNICs lies in the range of 1.973-2.025 Å. [f] The average Fe–S bond distance of (di)anionic $\{Fe(NO)_2\}^{10}$ DNICs lies in the range of 2.316-2.331 Å.

Table S4. Selected Bond Distances, Bond Angle, and $^{1}H/^{13}C$ NMR Signals for [Fe-(η^2-HCS_2)] and [M-(η^3-HCS_2)] Complexes.[a]

Complex	M–S (Å)	M–C[c] (Å)	C–S (Å)	∠S–C–S	^{1}H NMR (ppm)	^{13}C NMR (ppm)	Ref.
3	2.294 2.297	2.070	1.716 1.699	123.6	7.93	137.3	This work
[(L_1)Fe(η^2-HCS_2)(PMe_3)$_2$][b]	2.355 2.314	2.764	1.666 1.657	114.74	11.67	-	[25]
[(L_2)Fe(η^2-HCS_2)(PMe_3)$_2$][b]	2.356 2.310	2.689	1.675 1.624	118.75	11.52	205.6	[25]
[(depe)$_2$Fe(η^2-S_2CH)]$^{+}$ [b]	2.326 2.312	2.830	1.691 1.662	110.0	-	-	[26]
[(dppm)$_2$Fe(η^2-S_2CH)]$^{+}$ [b]	2.303 2.318	2.760	1.661 1.657	113.4	-	-	[27]
[$Mn_2(CO)_6$(μ-S_2CH)]$^{-}$	2.359 2.318	2.015	1.717 1.718	107.1	6.07	99.8	[28]
[(Cp^*)Mo(η^2-S_2CH_2)(η^3-S_2CH)]	2.402 2.391	2.223	1.720 1.719	121.8	5.90	67.8	[29]
[(Cp^*)W(η^2-S_2CH_2)(η^3-S_2CH)]	2.394 2.384	2.200	1.726 1.726	121.4	5.30	61.4	[29]

[a]All the crystallographically-characterized [Fe-(η^2-HCS_2)] and [M-(η^3-HCS_2)] complexes available on CCDC are included. [b]L_1 = 2,6-$F_2C_6H_3$-C(=NH)-C_6H_3-4-Cl, L_2 = C_6H_5-C(=NH)-C_6H_3-4-OMe, depe = bis(diethylphosphino)ethane, dppm = bis(diphenylphosphino)methane. [c]The average Fe–C bond distance of [Fe-(η^2-HCS_2)] complex lies in the range of 2.689-2.830 Å, whereas that of [M-(η^3-HCS_2)] complex lies in the range of 2.015-2.223 Å.

Table S5. Coordinates of Geometry-Optimized DNIC **1** with B3LYP/TZVP level.

Fe	0.70958300	0.03066400	-0.00096600
O	2.36893400	0.14952400	2.25839400
O	2.37703900	0.01160500	-2.25725700
N	1.57600300	0.10098000	1.37952300
N	1.58053900	0.01810700	-1.38032200
N	-0.96017400	1.40033600	-0.03022500
N	-0.84546600	-1.46669000	0.02985300
C	-2.15917400	0.58793800	-0.34319300
C	-2.09748500	-0.75286000	0.37049700
C	-1.10208700	2.06260600	1.28493400
C	-0.75910000	2.43888700	-1.06235400
C	-0.54878000	-2.49783400	1.04621200
C	-0.95422000	-2.12341200	-1.29084900
H	-3.08160000	1.11939600	-0.07154600
H	-2.18288200	0.43541000	-1.42239300
H	-2.98103700	-1.35598100	0.11949400
H	-2.10782500	-0.60100500	1.44994900
H	-1.94821100	2.76407300	1.28003200
H	-0.18599400	2.60350000	1.51049800
H	-1.25409800	1.32498800	2.06928300
H	-1.61462100	3.12730500	-1.10523200
H	-0.62113400	1.96723200	-2.03280800
H	0.14120700	3.00265200	-0.82775900
H	-1.34562400	-3.25346700	1.08989200
H	-0.43786300	-2.02887300	2.02134900
H	0.39114300	-2.98420400	0.79455700
H	-1.74044200	-2.89133900	-1.28234100
H	-0.00056900	-2.58465100	-1.53642300
H	-1.17862700	-1.39243000	-2.06383500

Table S6. Coordinates of Geometry-Optimized DNIC **1** with BP86/TZVP level.

Fe	0.69836300	-0.04137400	0.00121700
O	2.40127300	-0.05888000	2.26175000
O	2.39567400	-0.15302900	-2.26087600
N	1.58138700	-0.05260800	1.38796400
N	1.57773000	-0.10615400	-1.38648500
N	-0.82528600	1.46762100	-0.02187500
N	-0.97855300	-1.37960600	0.02178400
C	-2.09920200	0.78343700	-0.37685900
C	-2.18393800	-0.56103100	0.33381500
C	-0.93049100	2.11236300	1.31168600
C	-0.50963200	2.51296400	-1.02634000
C	-0.79534700	-2.43262000	1.05113500
C	-1.12320700	-2.03598500	-1.30303600
H	-2.97935100	1.40950900	-0.12692200
H	-2.10198300	0.63592900	-1.46693600
H	-3.11634100	-1.09039100	0.05282300
H	-2.20958100	-0.41232300	1.42351900
H	-1.70814700	2.90261200	1.30767500
H	0.04097300	2.55080300	1.56816000
H	-1.17494700	1.36731400	2.07806300
H	-1.30240700	3.28730000	-1.06149600
H	-0.40075100	2.04828200	-2.01373500
H	0.44569700	2.98151700	-0.76116600
H	-1.66705300	-3.11679000	1.08428600
H	-0.65413500	-1.96175700	2.03164400
H	0.10851500	-3.00624900	0.81310100
H	-1.98287900	-2.73624300	-1.30394300
H	-0.20094700	-2.58451700	-1.52802600
H	-1.26571800	-1.28354800	-2.08782500

Table S7. Coordinates of Geometry-Optimized DNIC **2** with B3LYP/TZVP level.

Fe	-0.00002000	0.31134600	0.00003900
N	1.36887300	-0.56476400	0.00002400
N	-1.36876100	-0.56498500	-0.00002600
O	2.21743000	-1.39931700	-0.00004100
O	-2.21723700	-1.39962200	-0.00003000
B	-0.00026800	2.49458400	-0.00000100
H	-0.00018200	1.71432100	1.02431700
H	0.00062000	1.71398100	-1.02424700
H	1.01433900	3.15210200	0.00001300
H	-1.01525300	3.15142500	-0.00051700

Table S8. Coordinates of Geometry-Optimized DNIC **2** with BP86/TZVP level.

Fe	-0.00000100	0.31487300	0.00000200
N	1.38693600	-0.56135900	0.00009300
N	-1.38692600	-0.56137600	-0.00014500
O	-2.25372300	-1.39649400	-0.00020100
O	2.25373300	-1.39647700	0.00012200
B	-0.00001400	2.47379100	0.00010500
H	0.00008000	1.68732600	-1.04227600
H	-0.00010700	1.68721900	1.04241000
H	-1.02315200	3.13635100	0.00004700
H	1.02311900	3.13635600	0.00023800

Table S9. Coordinates of Geometry-Optimized DNIC **3** with B3LYP/TZVP level.

Fe	0.32418800	-0.02655800	-0.00009000
N	1.19872700	-1.42251700	0.00032600
N	1.27365200	1.29152100	-0.00043100
O	2.20618600	-2.05139600	0.00039600
O	1.96095100	2.25102000	-0.00053400
C	-1.68734400	-0.60994400	0.00034400
S	-1.46976900	0.16638700	-1.52739000
S	-1.46935200	0.16742800	1.52747600
H	-1.92262700	-1.67089300	0.00073900

Table S10. Coordinates of Geometry-Optimized DNIC **3** with BP86/TZVP level.

Fe	0.29863200	-0.03759200	-0.00005000
N	1.19662000	-1.44881700	0.00013700
N	1.25426100	1.29766300	-0.00041500
O	2.26760400	-1.99917900	0.00041800
O	1.88973400	2.30870500	-0.00050800
C	-1.68540100	-0.62664700	0.00033100
S	-1.44163700	0.15605100	-1.53992200
S	-1.44121900	0.15717100	1.53999500
H	-1.94121300	-1.69241100	0.00080700

Reference

1. R. Wedmann, A. Zahl, T. E. Shubina, M. Durr, F. W. Heinemann, B. E. Bugenhagen, P. Burger, I. Ivanovic-Burmazovic and M. R. Filipovic, *Inorg. Chem.*, 2015, **54**, 9367-9380.
2. R. E. Stevens and W. L. Gladfelter, *Inorg. Chem.*, 1983, **22**, 2034-2042.
3. M.-C. Hung, M.-C. Tsai, G.-H. Lee and W.-F. Liaw, *Inorg. Chem.*, 2006, **45**, 6041-6047.
4. S. J. Schauer, D. P. Eyman, R. J. Bernhardt, M. A. Wolff and L. M. Mallis, *Inorg. Chem.*, 1991, **30**, 570-572.
5. G. M. Sheldrick and SADABS, *University of Gottingen: Gottingen, Germany*, 1996.
6. G. M. Sheldrick and SHELXTL, *Siemens Analytical X-ray InstrumentsInc.: Madison, WI,*, 1994.
7. M. J. Frisch, G. W. Trucks, H. B. Schlegel, G. E. Scuseria, J. R. C. M. A. Robb, G. Scalmani, V. Barone, B. Mennucci, G. A. Petersson, H. Nakatsuji, M. Caricato, X. Li, H. P. Hratchian, A. F. Izmaylov, J. Bloino, G. Zheng, J. L. Sonnenberg, M. Hada, M. Ehara, K. Toyota, R. Fukuda, J. Hasegawa, M. Ishida, T. Nakajima, Y. Honda, O. Kitao, H. Nakai, T. Vreven, J. A. Montgomery, Jr., J. E. Peralta, F. Ogliaro, M. Bearpark, J. J. Heyd, E. Brothers, K. N. Kudin, V. N. Staroverov, R. Kobayashi, J. Normand, K. Raghavachari, A. Rendell, J. C. Burant, S. S. Iyengar, J. Tomasi, M. Cossi, N. Rega, J. M. Millam, M. Klene, J. E. Knox, J. B. Cross, V. Bakken, C. Adamo, J. Jaramillo, R. Gomperts, R. E. Stratmann, O. Yazyev, A. J. Austin, R. Cammi, C. Pomelli, J. W. Ochterski, R. L. Martin, K. Morokuma, V. G. Zakrzewski, G. A. Voth, P. Salvador, J. J. Dannenberg, S. Dapprich, A. D. Daniels, Ö. Farkas, J. B. Foresman, J. V. Ortiz, J. Cioslowski, D. J. Fox and R. D. Gaussian 09, *Gaussian, Inc., Wallingford CT,*, 2009.
8. Mariusz Mitoraj and A. Michalak, *J. Mol. Model*, 2007, **13**, 347-355.
9. M. P. Mitoraj, M. Parafiniuk, M. Srebro, M. Handzlik, A. Buczek and A. Michalak, *J. Mol. Model*, 2011, **17**, 2337-2352.
10. A. Michalak, M. Mitoraj and T. Ziegler, *J. Phys. Chem. A*, 2008, **112**, 1933-1939.
11. M. P. Mitoraj, A. Michalak and T. Ziegler, *J. Chem. Theory Comput.*, 2009, **5**, 962-975.
12. T. Ziegler and A. Rauk, *Theor. Chim. acta*, 1977, **46**, 1-10.
13. S.-W. Yeh, C.-W. Lin, B.-H. Liu, C.-C. Tsou, M.-L. Tsai and W.-F. Liaw, *Chem. Eur. J.*, 2015, **21**, 16035-16046.
14. T. Z. E.J. Baerends, A.J. Atkins, J. Autschbach, O. Baseggio, D. Bashford, A. Bérces, F.M. Bickelhaupt, C. Bo, P.M. Boerrigter, L. Cavallo, C. Daul, D.P. Chong, D.V. Chulhai, L. Deng, R.M. Dickson, J.M. Dieterich, D.E. Ellis, M. van Faassen, L. Fan, T.H. Fischer, C. Fonseca Guerra, M. Franchini, A. Ghysels, A. Giammona, S.J.A. van Gisbergen, A. Goez, A.W. Götz, J.A. Groeneveld, O.V. Gritsenko, M. Grüning, S. Gusarov, F.E. Harris, P. van den Hoek, Z. Hu, C.R. Jacob, H. Jacobsen, L. Jensen, L. Joubert, J.W. Kaminski, G. van Kessel, C. König, F. Kootstra, A. Kovalenko, M.V. Krykunov, E. van Lenthe, D.A. McCormack, A. Michalak, M. Mitoraj, S.M. Morton, J. Neugebauer, V.P. Nicu, L. Noodleman, V.P. Osinga, S. Patchkovskii, M. Pavanello, C.A. Peeples, P.H.T. Philipsen, D. Post, C.C. Pye, H. Ramanantoanina, P. Ramos, W. Ravenek, J.I. Rodríguez, P. Ros, R. Rüger, P.R.T. Schipper, D. Schlüns, H. van Schoot, G. Schreckenbach, J.S.

Seldenthuis, M. Seth, J.G. Snijders, M. Solà, M. Stener, M. Swart, D. Swerhone, V. Tognetti, G. te Velde, P. Vernooijs, L. Versluis, L. Visscher, O. Visser, F. Wang, T.A. Wesolowski, E.M. van Wezenbeek, G. Wiesenekker, S.K. Wolff, T.K. Woo, A.L. Yakovlev, *ADF2018, SCM, Theoretical Chemistry, Vrije Universiteit, Amsterdam, The Netherlands*.

15. E. F. Pettersen, T. D. Goddard, C. C. Huang, G. S. Couch, D. M. Greenblatt, E. C. Meng and T. E. Ferrin, *J. Comput. Chem.*, 2004, **25**, 1605-1612.
16. L. J. Li, N. Reginato, M. Urschey, M. Stradiotto and J. D. Liarakos, *Can J Chem*, 2003, **81**, 468-475.
17. C.-H. Hsieh and M. Y. Darensbourg, *J. Am. Chem. Soc.*, 2010, **132**, 14118-14125.
18. J. L. Hess, C.-H. Hsieh, J. H. Reibenspies and M. Y. Darensbourg, *Inorg. Chem.*, 2011, **50**, 8541-8552.
19. C.-H. Hsieh, R. Pulukkody and M. Y. Darensbourg, *Chem. Comm.*, 2013, **49**, 9326-9328.
20. R. Pulukkody, S. J. Kyran, R. D. Bethel, C.-H. Hsieh, M. B. Hall, D. J. Darensbourg and M. Y. Darensbourg, *J. Am. Chem. Soc.*, 2013, **135**, 8423-8430.
21. F.-T. Tsai, P.-L. Chen and W.-F. Liaw, *J. Am. Chem. Soc.*, 2010, **132**, 5290-5299.
22. F.-C. Lo, Y.-C. Ho, P.-Y. Chang, G.-H. Lee, T.-S. Kuo, J.-L. Chen and C.-H. Chen, *Eur. J. Inorg. Chem.*, 2014, 3499-3509.
23. S.-W. Yeh, C.-W. Lin, Y.-W. Li, I.-J. Hsu, C.-H. Chen, L.-Y. Jang, J.-F. Lee and W.-F. Liaw, *Inorg. Chem.*, 2012, **51**, 4076-4087.
24. M.-C. Hung, M.-C. Tsai, G.-H. Lee and W.-F. Liaw, *Inorg. Chem.*, 2006, **45**, 6041-6047.
25. L. Wang, H. Sun, Z. Zuo, X. Li, W. Xu, R. Langer, O. Fuhr and D. Fenske, *Eur. J. Inorg. Chem.*, 2016, 5205-5214.
26. C. Bianchini, P. Innocenti, A. Meli, A. Orlandini and G. Scapacci, *J. Organomet. Chem.*, 1982, **233**, 233-246.
27. Y. Gao, D. G. Holah, A. N. Hughes, G. J. Spivak, M. D. Havighurst, V. R. Magnuson and V. Polyakov, *Polyhedron*, 1997, **1997**, 2797-2807.
28. B. Alvarez, S. García-Granda, Y. Jeannin, D. Miguel, J. A. Miguel and V. Riera, *Organometallics*, 1991, **10**, 3005-3007.
29. C. E. Rao, S. K. Barik, K. Yuvaraj, K. Bakthavachalam, T. Roisnel, V. Dorcet, J.-F. Halet and S. Ghosh, *Eur. J. Inorg. Chem.*, 2016, 4913-4920.